Assessment of spray drift potential reduction for hollow-cone nozzles: Part 2. LiDAR technique

Eduard Gregorio[a*], Xavier Torrent[a], Santiago Planas[a,b], Joan R. Rosell-Polo[a]

[a] Research Group in AgroICT & Precision Agriculture, Department of Agricultural and Forest Engineering, Universitat de Lleida (UdL)-Agrotecnio Center, Edifici CREA, c/ Pere de Cabrera s/n, 25001 Lleida, Spain

[b] Plant Health Services. Generalitat de Catalunya, Avda. Rovira Roure, 191, 25198, Lleida, Spain.

* Corresponding author. E-mail address: egregorio@eagrof.udl.cat (E. Gregorio).

Abstract

Pesticide spray drift poses health hazards to humans and causes a significant impact on the environment. In this work the capacity of an ad hoc light detection and ranging (LiDAR) system to differentiate spray nozzles according to their potential drift risk is evaluated for the first time. A total of 23 drift potential tests using 10 hollow-cone nozzles were carried out with the sprayer kept in a static position. Drift potential reduction (*DPR*) values of between 88.6% and 93.6% were obtained when comparing standard and drift reduction nozzle types. It was also possible to order different standard nozzle sizes according to their *DPR*. The LiDAR signal was correlated with several droplet size parameters measured by a phase Doppler particle analyzer (PDPA), being V_{100} the best indicator. In the four field tests that were performed, the LiDAR system was also able to differentiate between standard and drift reduction nozzles under real application conditions, obtaining a *DPR* of 56.7%. The results of this work demonstrate that the developed LiDAR system is an advantageous alternative for the assessment of drift potential reduction.

Keywords: light detection and ranging, pesticide drift, drift reduction, droplet size, pesticide spraying

Nomenclature

DPR	drift potential reduction (%)
DPR_{lidar}	drift potential reduction based on LiDAR measurements (%)
DPR_{V100}	drift potential reduction based on V_{100} (%)
DRN	drift reduction nozzle
D_{Vx}	volume diameter, indicates that the *x* (% of the spray volume) is in smaller droplets (µm)
PDPA	phase Doppler particle analyzer
S_{lidar}	normalized LiDAR signal
STN	standard nozzle
V_x	volume fraction of droplets smaller than *x* µm in diameter (%)

1. Introduction

During pesticide spraying operations, part of the product is carried out of the target area by the action of air currents, giving rise to spray drift. This is a primary source of pollution and presents significant risks to health and to the environment (EPA, 2018). Numerous studies have evaluated the exposure of spray drift on ecosystems (de Jong et al., 2008), on water bodies (Zhang et al., 2018), on agricultural workers (De Schampheleire et al., 2007) and on bystanders and residents (Butler Ellis et al., 2017b). In addition, drift can be transported long distances or can even occur once the application is completed (indirect drift). The amount, concentration and toxicity of the pesticide applied are major factors that affect the spray drift impacts (Damalas, 2015).

Spray drift is affected by a multitude of mechanisms including the meteorological conditions, the application technique, spray characteristics, the equipment used, the target crop and the operator skills (Gil and Sinfort, 2005; Heidary et al., 2014). It is essential to develop drift assessment methods that make it possible to understand these mechanisms (Felsot et al., 2010) and facilitate the application of more efficient mitigation measures (FOCUS, 2004). Such assessment methods

should also be able to classify each spraying technology according to their spray drift potential (Gil et al., 2015).

Among current assessment methods (Nuyttens et al., 2010), it is possible to distinguish between those based on the field measurement of spray drift under real application conditions (ISO 22866:2005), and those based on determining drift potential under controlled conditions, either through wind tunnels or using droplet size characteristics. With regard to field measurements, systematic measurements were taken in Germany (Ganzelmeier et al., 1995; Rautmann et al., 2001) and in the Netherlands (Holterman et al., 1997; Holterman et al., 2017), obtaining prediction models that allowed the establishment of a relationship between drift percentage and distance. It should be noted that these models respond to specific application conditions and cannot be directly extrapolated to other geographical environments with different weather conditions and crops (Bueno et al., 2017). Field spray drift studies are generally carried out using *in situ* collectors and tracers (Garcerá et al., 2017). These are complex, time-consuming and labor intensive experiments and the results are affected by meteorological factors (Gil et al., 2018; Otto et al., 2015; Torrent et al., 2017).

In laboratory tests, the aim is to evaluate the spray drift potential, which is defined as the percentage of the initial sprayed volume that is carried downwind as airborne spray (ISO 22856:2008). Drift potential can be evaluated by spraying with a nozzle placed inside a tunnel and measuring the resulting drift by using collectors (Ferguson et al., 2015; Nuyttens et al., 2009). Wind tunnels allow drift measurements to be taken in controlled and repeatable conditions. In this context, Butler Ellis et al. (2017a) studied the capacity to predict the spray drift reduction from the relationship between wind tunnel and field measurements. Despite these advantages, the limited dimensions of tunnels entail that complete spray drift studies cannot be performed. As an alternative to wind tunnel measurements, Balsari et al. (2007) developed a test bench for the drift potential assessment of boom sprayers (ISO 22401:2015). This test bench has been used to classify different nozzles and field crop sprayer application techniques on the basis of their drift

77 potential (Gil et al., 2014; Nuyttens et al., 2017) and has been recently contrasted with field spray
78 drift measurements (Grella et al., 2019).

79 Spray drift potential can also be indirectly evaluated from the droplet size distribution. It is widely
80 known that smaller droplets present a greater tendency to drift (Taylor et al., 2004). In this respect,
81 Zande et al. (2008) conducted a classification of different nozzles in four drift reduction classes
82 based on V_{100}. Determination of spay droplet size is usually carried out in the laboratory under
83 controlled conditions using laser light diffraction techniques or phase Doppler particle analyzers
84 (Miller, 2014). However, with these techniques only the nozzle is evaluated. It should also be
85 borne in mind that field measurements of spray drift using the same nozzles and working pressure
86 can vary by a factor of 10 due to weather conditions (Nuyttens, 2007).

87 The light detection and ranging (LiDAR) technique has also been used for drift measurement in
88 aerial spraying applications (Hiscox et al., 2006; Hoff et al., 1989; Stoughton et al., 1997). Unlike
89 passive collectors, which only provide punctual and time-integrated information, LiDAR systems
90 allow real-time range-resolved measurements of spray drift. The technique required is simple and
91 fast, since a single operator can carry out the LiDAR measurements without the need for further
92 chemical analyses. A good agreement between LiDAR and collector measurements has been
93 found in previous spray drift studies (Gregorio et al., 2014; Khot et al., 2011). Despite these
94 benefits, the currently available LiDAR systems are not suitable for drift measurements because
95 they are typically complex and expensive instruments designed for atmospheric research.

96 In order to overcome these limitations, the Research Group in AgroICT & Precision Agriculture
97 of the Universitat de Lleida has developed an ad hoc LiDAR system for the measurement of
98 pesticide spray drift (Gregorio et al., 2015). It is a compact, easily transportable and eye-safe
99 instrument, more affordable than conventional atmospheric LiDAR systems. The developed
100 prototype has been field tested (Gregorio et al., 2016), obtaining high coefficients of
101 determination (R^2>0.85) when comparing LiDAR measurements with tracer depositions in
102 ground collectors (ISO 22866:2005). The main objective of this work is to assess the capacity of

the system to differentiate spray nozzles according to their drift potential reduction (*DPR*). To this end, 23 drift potential tests and 4 field tests were carried out, where the effects of nozzle type and nozzle size were studied.

2. Materials and methods

2.1. Spray drift potential tests

Two types of spraying tests were carried out, drift potential tests and field measurements of the spray drift under real application conditions. The drift potential tests are described in this section, while the field tests will be presented in Section 2.2.

The drift potential tests were conducted at the School of Agrifood and Forestry Science and Engineering (lat. 41.6294770N, long. 0.5962083ºE, elev. 189 m) of the Universitat de Lleida, Spain. An air-assisted sprayer (Teyme Eolo 2091, Teyme Tecnología Agrícola SL, Torre-Serona, Spain) was used, which remained in static position throughout all these tests. Both in this experiment and in the field tests, the sprayed liquid was tap water. The LiDAR system was placed at a distance of 50 m from the sprayer (Fig. 1), thus ensuring a full overlap between the emitted laser beam and the receiver field of view (Measures, 1992). The LiDAR system was aimed almost horizontally, so the laser beam monitored the airborne spray drift at 6.5 m behind the sprayer.

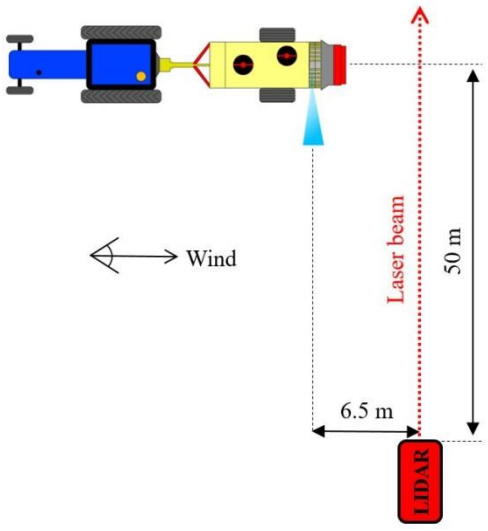

Fig. 1. Experimental layout for the spray drift potential tests.

As shown in Table 1, a total of 23 drift potential tests were conducted, completing between 3 and 5 repetitions per test (except for tests T4 and T13 with 2 repetitions). The measures were carried out in three different periods: autumn (November 11, 2015), winter (January 25, 2016) and summer (July 4, 2017). The goal of the autumn tests (T1 to T6) was to assess the capacity of the LiDAR system to distinguish the spray drift generated by two different types of hollow-cone nozzles: standard (STN) Albuz ATR (Solcera, Evreux, France), and drift reduction (DRN) Albuz TVI. These nozzles were tested at two working pressures (700 and 1000 kPa) and with two fan speeds. In winter (T7 to T13), a comparative study was made of seven STN of different sizes, at a pressure of 700 kPa. In all the autumn and winter tests, 5 nozzles on each side of the sprayer were used, and the laser pulse repetition frequency (i.e. the number of laser pulses emitted per second) was adjusted to 5 Hz. In these tests, the sequence followed was: (t=0 s) laser emission starts; (t=10 s) spraying starts; (t=25 s) end of spraying; (t=80 s) end of laser emission.

In the summer tests, the comparison between STN of different sizes was repeated (T14 to T20) and three additional tests with DRN were performed (T21 to T23). In all these tests, only 5 nozzles on one side of the sprayer were used, the spraying time was 30 s (from t=10 s to t=40 s), and the laser pulse repetition frequency was reduced to 1 Hz.

139 **Table 1.** Description of the spray drift potential tests.

Test	Date	Num. of repetitions	Pulse repetition frequency (Hz)	Nozzle model	Pressure (kPa)	Num. of nozzles	Fan velocity	Spraying duration (s)	Sprayed volume (L)
T1		3		ATR 80 Grey	700		Low		4.400
T2		4		TVI 8003 Blue	700		Low		4.575
T3		3		ATR 80 Grey	700		High		4.400
T4	11/11/15	2	5	TVI 8003 Blue	700	10	High	15	4.575
T5		3		ATR 80 Grey	1000		Low		5.200
T6		3		TVI 8003 Blue	1000		Low		5.475
T7		3		ATR 80 Lilac	700		Low		1.050
T8		3		ATR 80 Brown	700		Low		1.400
T9		4		ATR 80 Yellow	700		Low		2.150
T10	1/25/16	4	5	ATR 80 Orange	700	10	Low	15	2.925
T11		4		ATR 80 Red	700		Low		4.050
T12		4		ATR 80 Grey	700		Low		4.400
T13		2		ATR 80 Green	700		Low		5.225
T14		5		ATR 80 Lilac	700		Low		1.050
T15		5		ATR 80 Brown	700		Low		1.400
T16		5		ATR 80 Yellow	700		Low		2.150
T17	7/4/17	5	1	ATR 80 Orange	700	5	Low	30	2.925
T18		5		ATR 80 Red	700		Low		4.050
T19		5		ATR 80 Grey	700		Low		4.400
T20		5		ATR 80 Green	700		Low		5.225
T21		5		TVI 8003 Blue	700		Low		4.575
T22	7/4/17	5	1	TVI 8002 Yellow	700	5	Low	30	3.050
T23		5		TVI 8001 Orange	700		Low		1.525

140

141 *2.2. Field tests*

142 The goal of this second experiment was to establish guidelines for performing field drift tests with
143 the developed LiDAR system. The tests were carried out on July 12 and 18, 2017, at a peach
144 orchard owned by the Institute of Agrifood Research and Technology (IRTA) in Gimenells (lat.
145 41.3911111N, long. 0.2312811E, elev. 259 m) located 25 km from Lleida, Spain. The same

146 sprayer was used as in the drift potential tests, moving 50 m along the external alley (Fig. 2). The
147 LiDAR system was aimed horizontally with the laser beam parallel to the first tree row, at a
148 distance of 6.5 m downwind from its longitudinal axis. The minimum separation between the
149 LiDAR system and the sprayer was 60 m (at the end of the sprayer displacement), thus ensuring
150 full overlap.

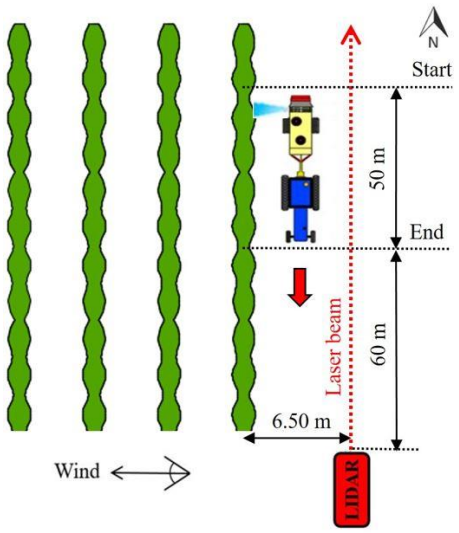

151

152 **Fig. 2.** Experimental layout for the field tests. The terms "Start" and "End" refer, respectively, to the positions at
153 which the sprayer started and ended its displacement.

154 One of the main difficulties for the LiDAR measurement of spray drift is the presence of dust
155 suspended in the air as a consequence of fan action and sprayer displacement, which can distort
156 the resulting signal (Gregorio et al., 2018). To assess this effect, on July 12 dust raised by the
157 tractor and the sprayer was measured under dry soil conditions (T1) and, after watering the soil,
158 under wet soil conditions (T2). Three repetitions of each test were completed. In these tests, the
159 tractor and sprayer were displaced along the external alley with the fan on but without spraying.

160 On July 18, two spraying tests (F3 and F4) were conducted under wet soil conditions. The STN
161 ATR 80 Grey and the DRN TVI 8003 were compared (Table 2). The sprayer moved along the
162 external alley with the fan off. The first tree row was sprayed using 5 nozzles on one side at a
163 working pressure of 1000 kPa. In all field tests, the LiDAR system measured for 90 s, with a laser
164 pulse repetition frequency of 1 Hz. This time period includes the path of the sprayer along the

alley, as well as an additional interval to measure the remaining spray drift suspended in the air after the end of the application.

Table 2. Description of the field tests.

Test	Date	Num. of repetitions	Ground state	Nozzle model	Pressure (kPa)	Num. of nozzles	Fan velocity	Forward speed (km h^{-1})	Volume rate (l·ha^{-1})
F1	7/12/17	3	Dry	-	-	-	Low	5.5	-
F2			Wet						
F3	7/18/17	3	Wet	ATR 80 Grey	1000	5	Low	5.5	334
F4			Wet	TVI 8003 Blue					351

2.3. LiDAR system

The operation of the LiDAR system is based on the emission of short laser pulses (6 ns) and the reception of the signal backscattered by the target, which in this case are drift clouds. From the time elapsed between emission and reception (*time-of-flight*), it is possible to determine the distance at which the target is located. The intensity of the backscattered signal gives us information about the cloud concentration. In emission, the system consists of an erbium-doped glass laser with a wavelength of 1534 nm and 3 mJ of energy per pulse. Eye-safety is ensured thanks to the combination of this wavelength with a beam expander. The backscattered energy is captured by a reflector telescope with an aperture of 80 mm, and through a set of optics it is focused to an APD optoelectronic receiver. This photodetector module is responsible for converting the received light into an electrical signal.

As shown in Fig. 3, the optical head, comprised of the emitting and receiving subsystems, is held by means of a pan & tilt unit and a tripod. The pan & tilt unit allows movements in azimuth and elevation, providing scanning capability. The electrical signal at the photodetector output is digitized by using an analogue-to-digital converter (ADC) and directed to a computer where it can be displayed in real-time. An ad hoc LabView-based software has been developed that allows not only visualization of the LiDAR measurements but also data storage and full control of the instrument. The LiDAR system has a modular configuration to facilitate transportation and

assembly. The system was designed for the measurement of spray drift clouds up to 500 m, although solid targets located further than 2 km have been experimentally detected. Its range resolution is equal to 2.4 m, and the time resolution is adjustable up to a maximum of 0.1 s. A complete description of this LiDAR system can be found in Gregorio et al. (2015).

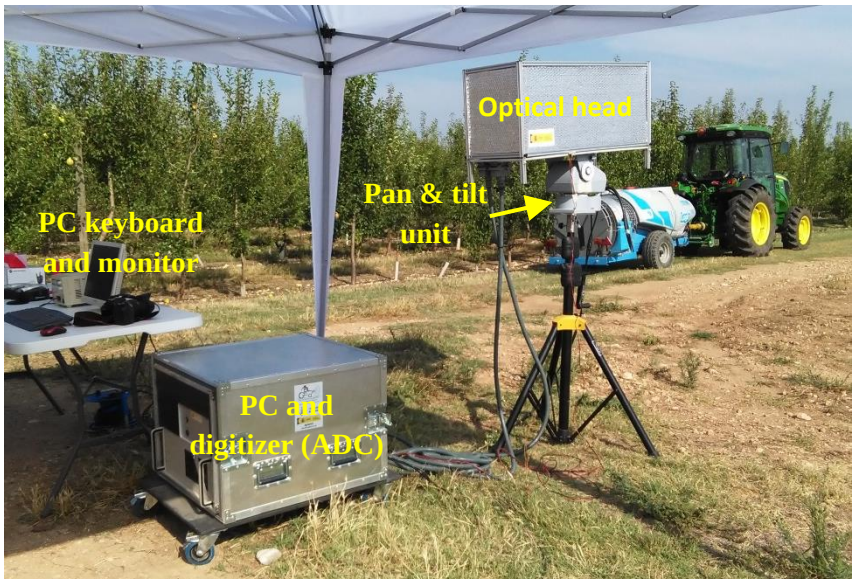

Fig. 3. Picture of the LiDAR system setup during the field tests. The sprayer is shown in the background.

2.4. Nozzle characteristics

A total of 10 Albuz hollow-cone nozzles were used in the tests. Table 3 presents, for each nozzle, its typology (STN or DRN), the working pressure considered, the main droplet size parameters (D_{V10}, D_{V50}, D_{V90}, V_{100} and V_{200}) and the flow rate. D_{V10}, D_{V50} (or volume median diameter) and D_{V90} correspond to the diameter of the drop below which are, respectively, 10%, 50%, and 90% of the total spray volume. V_{100} and V_{200} are the percentage in volume represented by droplets with a diameter less than 100 µm and 200 µm, respectively. Droplet size distribution was measured at IRSTEA (Montpellier, France) using a phase Doppler particle analyzer (PDPA, Dantec, Denmark) according to the ISO 25358:2018, as detailed in Part 1.

Table 3. Characteristics of the tested nozzles.

Nozzle		Pressure	D_{V10}	D_{V50}	D_{V90}	V_{100}	V_{200}	Flow rate
Model	**Type**	**(kPa)**	**(µm)**	**(µm)**	**(µm)**	**(%)**	**(%)**	**(L min^{-1})**
ATR 80 Lilac			57.2	95.3	144.1	54.9	99.1	0.420
ATR 80 Brown			61.7	105.9	158.1	44.3	97.7	0.560
ATR 80 Yellow			62.3	113.9	181.4	38.1	93.6	0.860
ATR 80 Orange	STN	700	67.9	125.4	196.5	30.0	90.8	1.170
ATR 80 Red			74.3	139.0	226.3	23.0	83.3	1.620
ATR 80 Grey			75.2	144.2	240.8	21.9	79.4	1.760
ATR 80 Green			79.3	151.5	254.0	19.0	75.7	2.000
TVI 8001 Orange			279.3	552.6	841.5	0.3	3.4	0.610
TVI 8002 Yellow	DRN	700	287.6	534.5	813.2	0.2	2.9	1.220
TVI 8003 Blue			270.1	493.0	786.0	0.3	3.5	1.830
ATR 80 Grey	STN	1000	70.9	132.9	219.4	26.2	85.8	2.080
TVI 8003 Blue	DRN	1000	277.8	509.7	810.7	0.3	3.3	2.190

2.5. Meteorological measurements

The main meteorological conditions (temperature, relative humidity, wind speed and wind direction) were recorded using a compact ultrasonic weather station (WXH220 model, Airmar Technology Corporation, Milford, NH, USA). The station was placed 20 m from the sprayer, at 6 m height above the ground. The acquisition frequency was 1 Hz. Table 4 shows a summary by date of the prevailing meteorological conditions during the tests, indicating the maximum and minimum values of each of the variables recorded (temperature, relative humidity, and wind speed). The wind direction remained in all tests within a range of ±30º from the perpendicular of the laser beam direction, as indicated in Figs. 1 and 2.

Table 4. Summary of the meteorological conditions during the tests. Data is presented by day.

Tests	Date	Temperature (ºC)		Relative humidity (%)		Wind speed (m s^{-1})	
		Min	Max	Min	Max	Min	Max
T1 – T6	11/11/15	11.80	12.20	88.5	91.0	0.65	0.80
T7 – T13	1/25/16	9.70	10.95	36.0	49.1	0.90	1.00
T14 – T23	7/4/17	30.06	35.29	33.0	52.0	1.13	2.01
F1 – F2	7/12/17	30.60	32.40	41.0	45.5	3.08	5.24
F3 – F4	7/18/17	31.50	32.20	34.0	36.5	7.00	7.74

2.6. LiDAR theoretical basis

The received LiDAR signal was background-subtracted and range-corrected. To determine the background signal, measurements corresponding to the 10 s prior to the beginning of the spraying (pre-calibration) were averaged. This background signal includes the solar component, as well as the backscatter due to molecules (Rayleigh scattering) and aerosols (Mie scattering) present in the atmosphere. Since the LiDAR signal depends inversely on the square of the distance (Wandinger, 2005), the received signal was multiplied by this factor in order to compare measurements corresponding to different ranges. The range-corrected background-subtracted LiDAR signal $S(r,t)$ received from a distance r at a time t is given in its simplified form by

$$S(r,t) = K \cdot \beta(r,t) \cdot T(r,t)\ , \quad (1)$$

where: K is the system constant and depends on the characteristics of the instrument used; $\beta(r,t)$ is the atmospheric backscattering coefficient, which describes the intensity of the backscattered light and depends on the particle number concentration in the monitored volume as well as on the particle backscattering cross section (related to the particle size distribution); and $T(r,t)$ is the transmissivity term, which indicates the light that is lost in the round trip to r. In the tests presented in this work, the transmissivity takes values close to one since the monitored spray drift clouds present a low optical density. A full overlap factor is also assumed in this expression.

To be able to quantify the spray drift generated in a test, the integrated LiDAR signal, S_{Int}, is defined. This fulfills a role similar to the spray drift potential defined by the ISO 22856:2008 standard. In each test, S_{Int} is calculated by integrating the range-corrected background-subtracted LiDAR signal $S(r,t)$ over the considered range of distances (R_{min}, R_{max}) and throughout the duration of the test (t_{min}, t_{max}). To allow comparisons between LiDAR measurements from different tests, the integrated signal is corrected taking into account the total sprayed volume and the laser pulse repetition frequency, obtaining

$$S_{Int}=\frac{1}{PRF\cdot V_s}\int_{t_{min}}^{t_{max}}\int_{R_{min}}^{R_{max}} S(r,t)\,drdt, \tag{2}$$

where PRF is the laser pulse repetition frequency and $V_s=\sum_{i=1}^{n} q_i \cdot t_a$ is the total sprayed volume, with q_i the flow rate per nozzle, n the number of nozzles, and t_a the spraying duration.

To avoid dependence on the system constant K, a normalized LiDAR signal S_{lidar} is used in this work. This parameter is expressed in per unit (p.u.), and can be calculated by dividing the integrated LiDAR signal, $S_{Int,C}$, of the spray drift test to be evaluated (candidate test) by the integrated LiDAR signal corresponding to the reference test, $S_{Int,R}$

$$S_{lidar}=\frac{S_{Int,C}}{S_{Int,R}}. \tag{3}$$

From the integrated LiDAR signal, S_{Int}, it is also possible to define the LiDAR-based drift potential reduction DPR_{lidar} (%), that is given by

$$DPR_{lidar}=\left(1-\frac{S_{Int,C}}{S_{Int,R}}\right)\cdot 100. \tag{4}$$

DPR_{lidar} is expressed as a percentage and allows evaluation of the capacity of the application equipment to reduce spray drift in relation to the reference sprayer.

2.7. Data analysis

The *DPR* was also calculated from the drop size measurements conducted with the PDPA. For this calculation, the parameter DPR_{V100} was used, which allows evaluation of the drift reduction

offered by a nozzle, called the candidate (C), with respect to a nozzle established as reference (R), in accordance with the following expression proposed by Zande et al. (2008),

$$DPR_{V100} = \left(1 - \frac{(V_{100})_C}{(V_{100})_R}\right) \cdot 100\ , \quad (5)$$

where $(V_{100})_C$ and $(V_{100})_R$ are the percentage of volume of droplets having a diameter smaller than 100 μm for the candidate and reference nozzles, respectively.

One-way analyses of variance (ANOVA) were performed to assess the effect of the nozzle size on the integrated LiDAR signal. In case of significant differences, multiple comparisons were carried out using the HSD Tukey test. Moreover, linear correlation coefficients of Pearson were obtained to check the relationship between the normalized LiDAR signal S_{lidar} and different droplet size parameters (D_{V10}, D_{V50} D_{V90}, V_{100} and V_{200}). The statistical analyses were carried out using JMP Pro 12 (SAS Institute Inc., Cary, NC, 1989-2007 for Windows), while the LiDAR signal processing was made with Matlab® (R2018a, Math Works Inc., Natick, Massachusetts, USA).

3. Results

3.1. Effect of nozzle type

The range-time intensity (RTI) plots of Fig. 4 show the time and distance evolution of the backscattered LiDAR signal corresponding to four tests (T1, T2, T5 and T6) carried out in autumn. Two nozzle types of similar flow rate (STN ATR 80 Grey and DRN TVI 8003 Blue) were compared at two different pressures (700 and 1000 kPa). It can be seen that the DRN (Fig. 4c,d) presents a signal an order of magnitude lower than the STN (Fig 4a,b) for both working pressures. In these graphs, two clouds can also be distinguished, corresponding to each side of the sprayer.

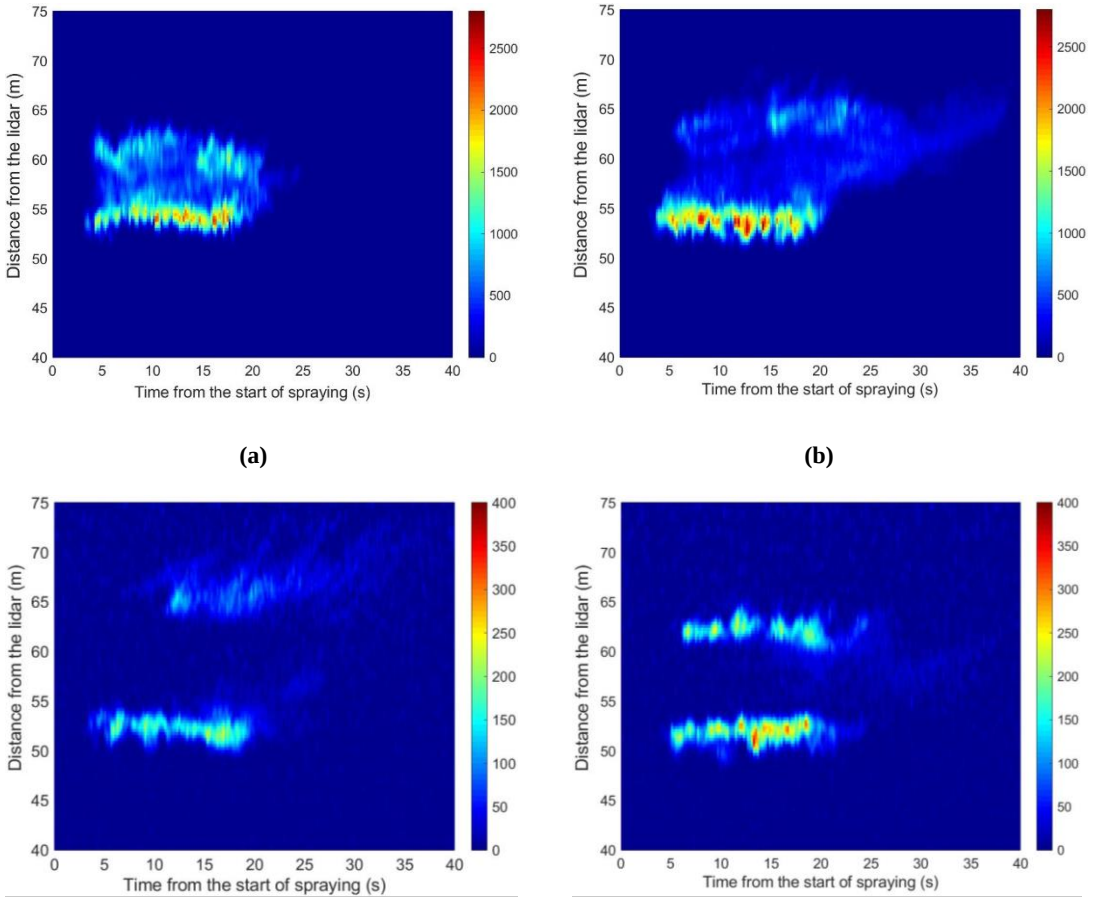

Fig. 4. RTI plots comparing nozzle type effect at two working pressures. (a) Test T1: ATR 80 Grey at 700 kPa; (b) Test T5: ATR 80 Grey at 1000 kPa; (c) Test T2: TVI 8003 Blue at 700 kPa; (d) Test T6: TVI 8003 Blue at 1000 kPa. Temporal resolution of 0.2 s and range resolution of 2.4 m. Color bar represents range-corrected backscattered signal (arbitrary units: a.u.). Signal range in (a-b) is 0-2750 a.u.; in (c-d) is 0-400 a.u.

An alternative way to represent the range-corrected LiDAR signal is through range profiles (Fig. 5a) and time profiles (Fig. 5b). The range profiles are obtained by time integration of $S(r,t)$ and normalizing (dividing) the resulting signal by the laser pulse repetition frequency and by the total sprayed volume. Similarly, the time profiles are calculated by distance integration, although in this case the signal is only normalized by the total sprayed volume, since the value of the accumulated signal at each time t does not depend on the laser pulse repetition frequency.

Fig. 5a shows the results of nozzle size comparison tests (STN vs. DRN) carried out in summer at a pressure of 700 kPa. The pairs of nozzles compared were: ATR 80 Brown and TVI 8001 Orange (T15, T23), ATR 80 Orange and TVI 8002 Yellow (T17, T22), ATR 80 Grey and TVI

296 8003 Blue (T19, T21). As in the autumn comparison (Fig. 4), a difference in intensity signal
297 between the two nozzle types is clearly observed. The presence of a single peak in the graphs of
298 Fig. 5 is because, in the summer tests, only the nozzles on one side were operating.

299 Fig. 5b shows again the tests of the previous RTI plots, but in this case represented in the form of
300 time profiles of the LiDAR signal. This figure allows to study how the signal was extinguished
301 once the application finished. It can be seen that in the tests with the DRN (at 700 and 1000 kPa),
302 and also with the STN at a working pressure of 700 kPa, cloud extinction occurred between 10
303 and 15 s after the end of the spraying. In contrast, when increasing the pressure of the STN to
304 1000 kPa, the extinction took about 30 s.
305

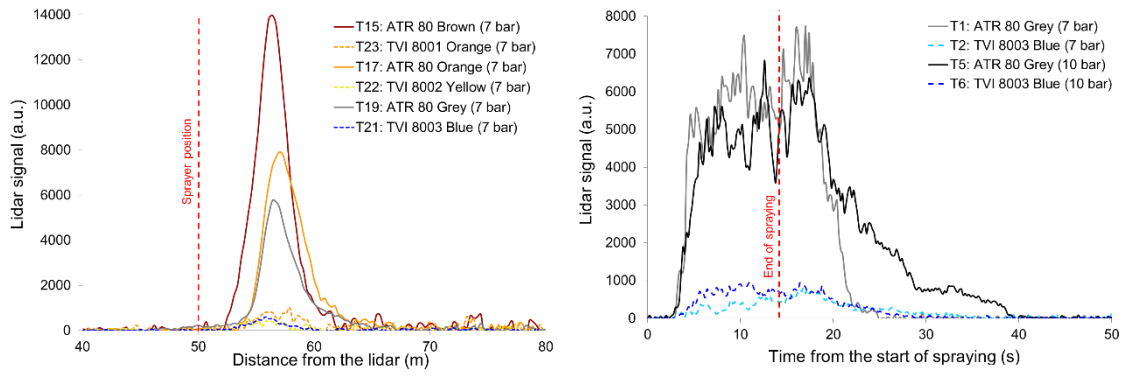

(a) **(b)**

306 **Fig. 5.** Comparison of nozzle type and pressure effects. (a) Range profile of range-corrected LiDAR returns (normalized
307 by the laser pulse repetition frequency and the total sprayed volume). Tests compared: T15 vs. T23, T17 vs. T22, T19
308 vs. T21. (b) Time profile of range-corrected LiDAR returns (normalized by the total sprayed volume). Tests T1, T2,
309 T5 and T6.
310

311 To quantitatively assess the effect of nozzle type, the normalized LiDAR signal S_{lidar} (reference
312 test: T1) was used, as well as the spray drift potential reduction (DPR_{V100} and DPR_{lidar}, defined in
313 Sect. 2.6 and 2.7) for each pair of nozzles (STN, DRN) with similar flow rates (Table 5). The
314 resulting S_{lidar} values indicate a 7-16-fold reduction of drift potential when comparing DRN to
315 STN. In terms of drift potential reductions, DPR_{V100} values of between 98.76% and 99.44%, and
316 DPR_{lidar} values of between 86.55% and 93.56%, were obtained.

317 **Table 5.** *DPR* values (%) for nozzle type comparisons (STN vs. DRN). S_{lidar} (per unit) is referred to test T1.

Test	Date	Nozzle model	Pressure (kPa)	Fan velocity	S_{lidar} (p.u.)	DPR_{V100} (%)	DPR_{lidar} (%)
T1	11/11/15	ATR 80 Grey	700	Low	1.000	0	0
T2		TVI 8003 Blue			0.114	98.76	88.57
T3	11/11/15	ATR 80 Grey	700	High	0.684	0	0
T4		TVI 8003 Blue			0.092	98.76	86.55
T5	11/11/15	ATR 80 Grey	1000	Low	1.047	0	0
T6		TVI 8003 Blue			0.129	98.92	87.70
T19	7/4/17	ATR 80 Grey	700	Low	0.855	0	0
T21		TVI 8003 Blue			0.066	98.76	92.25
T17	7/4/17	ATR 80 Orange	700	Low	1.172	0	0
T22		TVI 8002 Yellow			0.075	99.19	93.56
T15	7/4/17	ATR 80 Brown	700	Low	1.868	0	0
T23		TVI 8001 Orange			0.160	99.44	91.46

318

319 *3.2. Effect of nozzle size*

320 This section presents the results obtained when comparing different sizes of STN (Albuz ATR)
321 at a working pressure of 700 kPa. Fig. 6a shows, for some of the sizes studied (summer tests), the
322 range profile of the LiDAR signal, while in Fig. 6b the time profiles (winter tests) can be seen.
323 The results clearly show that the lower the size, the higher the LiDAR signal and, therefore, the
324 greater the drift potential. This same behavior can be observed in Fig. 7 which shows the
325 integrated LiDAR signal corresponding to the STN sizes tested in winter (T7-T13) and summer
326 periods (T14-T20). Moreover, it is noted the existence of significant differences ($p\text{-}value<0.05$)
327 in the LiDAR signal respect to the nozzle size for both periods. In winter tests, the highest drift
328 potential corresponds to Lilac and Brown sizes. By contrast, statistically significant differences
329 where observed between these two and the Yellow size, with a lower drift potential. A third group
330 is made up of Grey and Green sizes, which presented the lowest drift potential of all tested STN
331 nozzles. It is not obvious to classify the Orange and Red sizes because no significant differences

with respect to Yellow and Green were obtained. A similar trend was observed for the summer tests, except that the Grey size cannot be distinguished from the Red and Green.

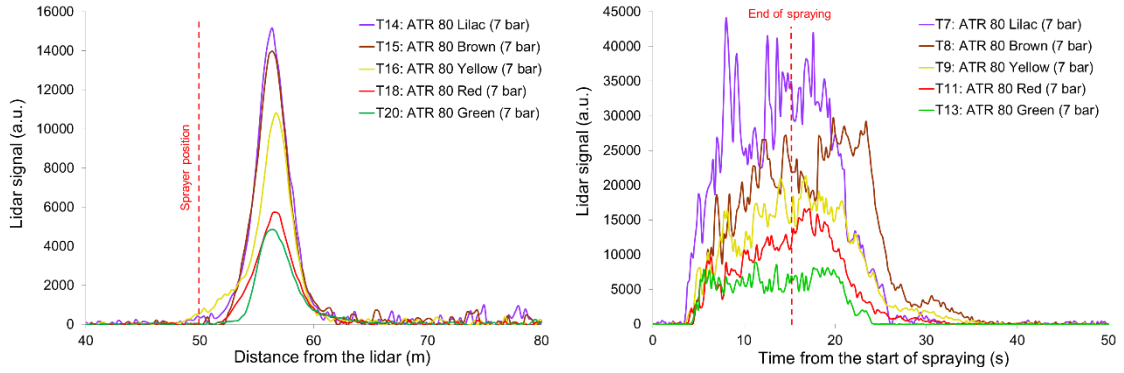

(a) **(b)**

Fig. 6. Nozzle size comparison for the STN type (Albuz ATR) at 700 kPa. (a) Range profile of LiDAR returns (summer tests: T14, T15, T16, T18 and T20); (b) Time profile of LiDAR returns (winter tests: T7, T8, T9, T11 and T13). LiDAR signal has been normalized by the total sprayed volume in (a) and (b), and also by the laser pulse repetition frequency in (a).

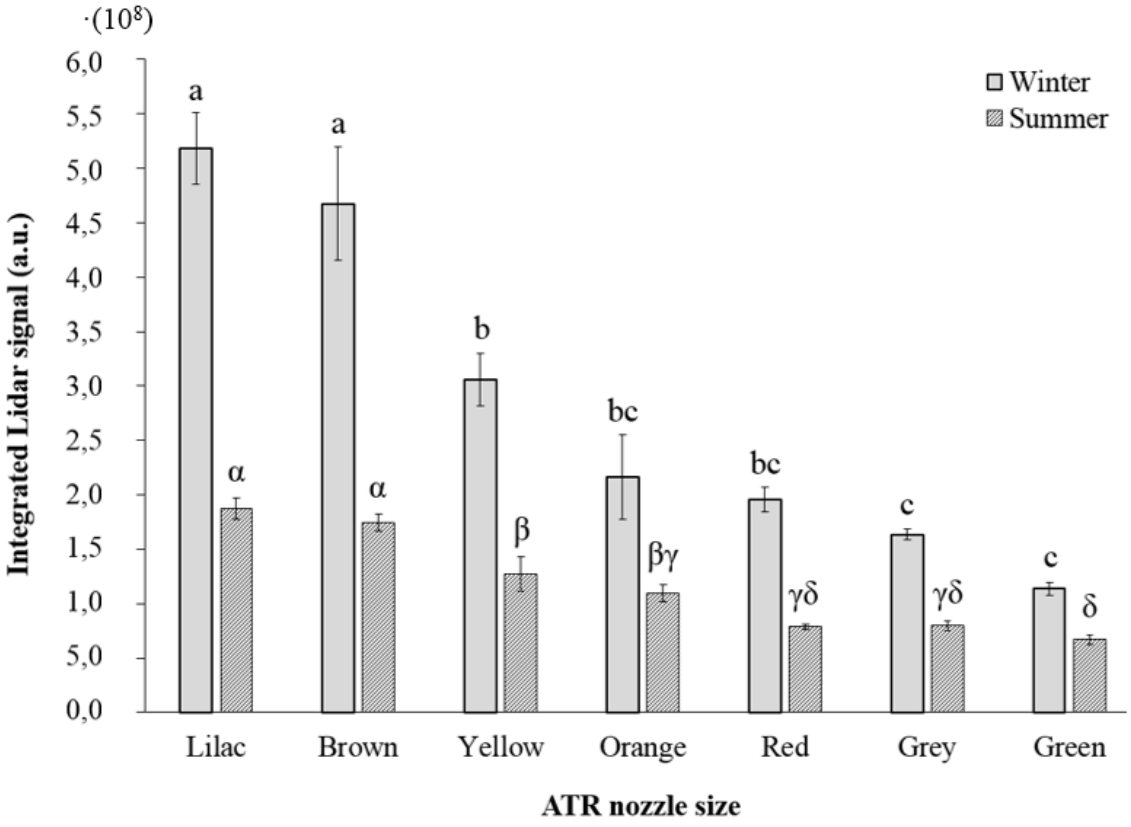

Fig. 7. Integrated LiDAR signal (mean with SE) for different ATR nozzle sizes (winter tests: T7-T13; summer tests: T14-T20). Also, results from the multiple comparison test are shown with Latin and Greek letters, where different letters indicate statistically significant differences.

As in the nozzle type comparison, the normalized LiDAR signal, S_{lidar}, values (reference test: T1) were computed. The DPR_{V100} and DPR_{lidar} were also determined, taking as reference the ATR 80 Lilac nozzle. Table 6 allows a quantitative comparison between the results obtained for different nozzle sizes in the winter and summer tests.

Table 6. *DPR* values (%) for nozzle size comparison (reference: ATR 80 Lilac). Winter: tests T7-T13; Summer: tests T14-T20. S_{lidar} (per unit) is referred to test T1.

Nozzle	Test		S_{lidar} (p.u.)		DRP_{V100} (%)	DRP_{lidar} (%)	
	Winter	Summer	Winter	Summer		Winter	Summer
ATR 80 Lilac	T7	T14	5.547	2.007	0	0	0
ATR 80 Brown	T8	T15	5.002	1.868	19.18	9.84	6.91
ATR 80 Yellow	T9	T16	3.274	1.359	30.55	40.98	32.27
ATR 80 Orange	T10	T17	2.314	1.172	45.34	58.29	41.61
ATR 80 Red	T11	T18	2.094	0.841	58.06	62.25	58.11
ATR 80 Grey	T12	T19	1.750	0.855	60.07	68.46	57.42
ATR 80 Green	T13	T20	1.217	0.716	65.43	78.06	64.33

The *DPR* values increased with nozzle size in all cases, regardless of the methodology used (PDPA, LiDAR), both for the winter and summer tests (Fig. 8). It should be mentioned, as the only exception, that the ATR 80 Grey nozzle (in the summer tests) presented a DPR_{lidar} slightly lower than that of the ATR 80 Red nozzle (immediately lower size).

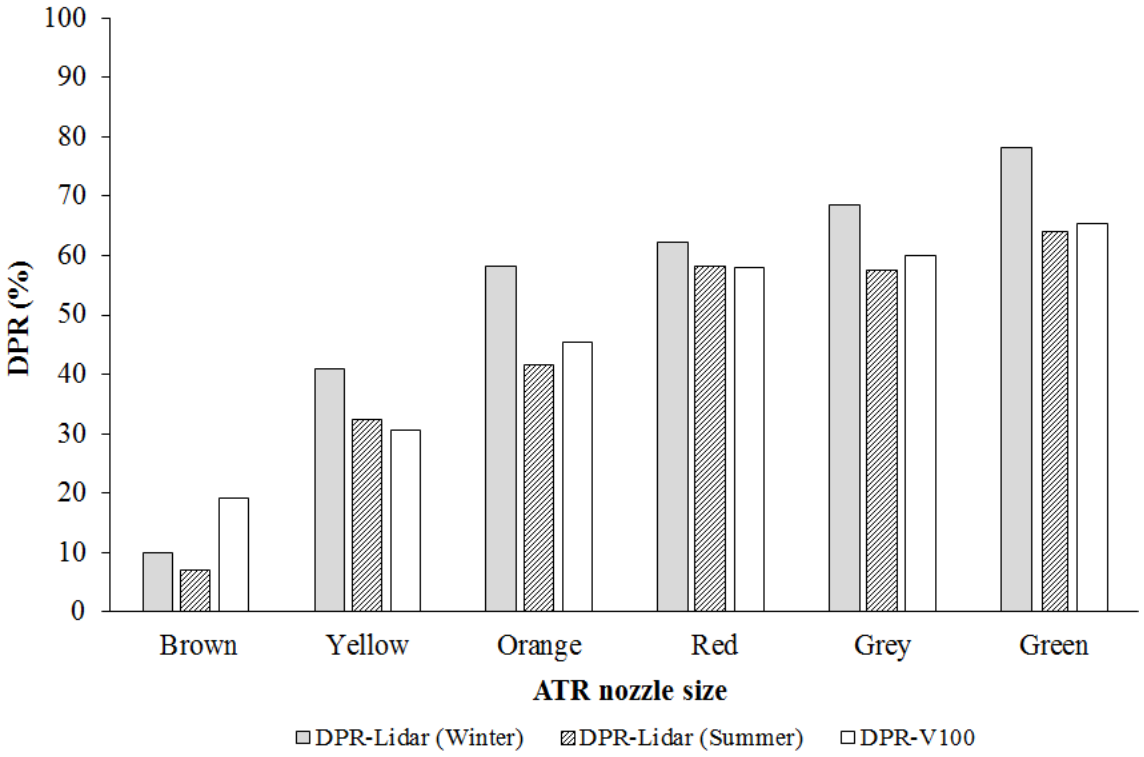

Fig. 8. Nozzle size comparison (reference: ATR 80 Lilac). For each nozzle, DPR_{lidar} (grey) obtained in winter tests (T7-T13), DPR_{lidar} (striped) obtained in summer tests (T14-T20), and DPR_{V100} (white), are shown.

3.3. Comparison between LiDAR and indirect methods

Table 7 shows the resulting linear correlation coefficients of Pearson between S_{lidar} and different droplet size parameters (D_{V10}, D_{V50}, D_{V90}, V_{100} and V_{200}) when considering the following sets: autumn and winter tests (T1-T13); 2) summer tests (T14-T23); all the tests (T1-T23). V_{100} presented the highest values for all the three sets, followed by the V_{200} parameter. Of the three sets of tests, the highest coefficient of Pearson (R=0.967) was obtained for the summer tests, as these were carried out on the same day whereas the autumn and winter tests were carried out in two different periods.

Table 7. Linear correlation coefficients of Pearson (*R*) between normalized LiDAR signal S_{lidar} and droplet size parameters. First column includes tests carried out in autumn and winter (T1-T13); second column corresponds to summer tests (T14-T23); last column includes all the tests.

	Tests T1-T13	**Tests T14-T23**	**Tests T1-T23**
D_{V10} (µm)	0.606	0.813	0.591
D_{V50} (µm)	0.628	0.822	0.602
D_{V90} (µm)	0.647	0.837	0.616
V_{100} (%)	0.906	0.967	0.765
V_{200} (%)	0.685	0.865	0.643

To verify the robustness of the relationship between S_{lidar} and V_{100}, a correlation analysis was conducted between the DPR_{lidar} and DPR_{V100} values by considering the results of all comparisons (Table 5 and Table 6) without distinguishing between nozzle type, nozzle size or meteorological conditions. In this analysis, all the *DPR* values were considered together because it is a relative parameter. A high correlation coefficient of Pearson between DPR_{lidar} and DPR_{V100} was obtained (R=0.956).

The LiDAR results were also compared with those obtained in wind tunnel tests carried out by Torrent et al. (2019). Fig. 9 shows the *DPR* values based on LiDAR and wind tunnel measurements (sedimenting and airborne depositions) for 3 STN (ATR 80 Yellow, ATR 80 Orange and ATR 80 Red) and 1 DRN (TVI 8002 Yellow). All of these nozzles were tested at 700 kPa. The *DPR* values were determined using ATR 80 Lilac as the reference nozzle. Although these results show a certain difference in magnitude, the same trend can be observed. Thus, it can be seen how *DPR* increases with nozzle size for both methods. It should be noted that the wind tunnel measurements were performed under controlled conditions unlike the LiDAR tests.

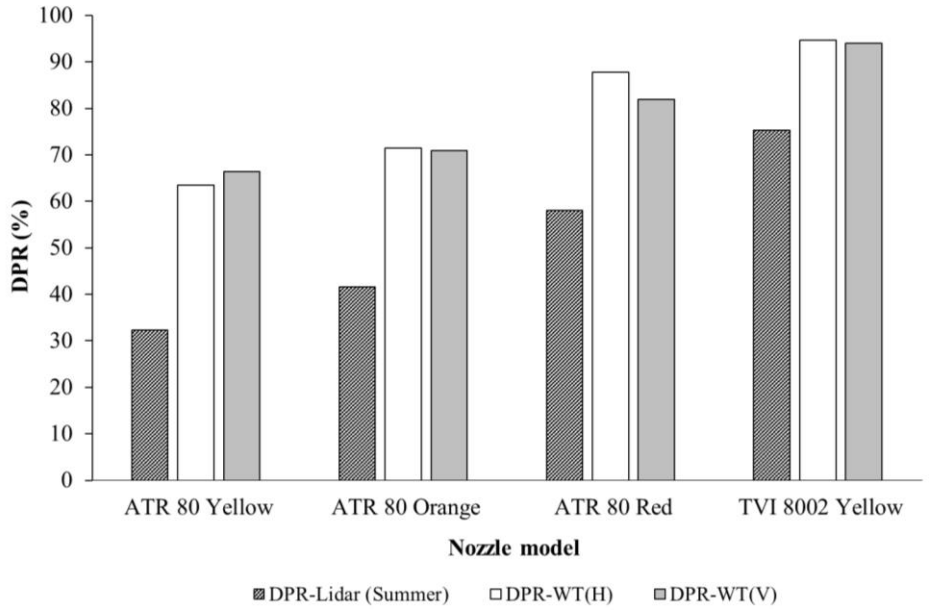

391

392 **Fig. 9.** Comparison between *DPR* values based on LiDAR and wind tunnel methods (sedimenting, H, and airborne
393 depositions, V) for four different nozzle models. Reference nozzle: ATR 80 Lilac at 700 kPa.

394

395 *3.4. Field tests*

396 Fig. 10 shows the RTI plots corresponding to the tests carried out in the field. In a first phase, the
397 effect of dust suspended in the air was studied in two different situations: dry soil (test F1) and
398 wet soil (F2). Under dry soil conditions, the terrain characteristics (bare soil), together with the
399 high temperature (>30ºC) and low humidity (<50%) prevailing during the tests (Table 4), favored
400 the raise of a large amount of dust. Therefore, the LiDAR signal due to dust (Fig. 10a) was intense
401 enough to distort the spray drift assessment. In contrast, under wet soil conditions (Fig. 10b), the
402 signal due to dust sharply decreased (76.76% reduction), allowing the completion of spray drift
403 tests without significant alterations.

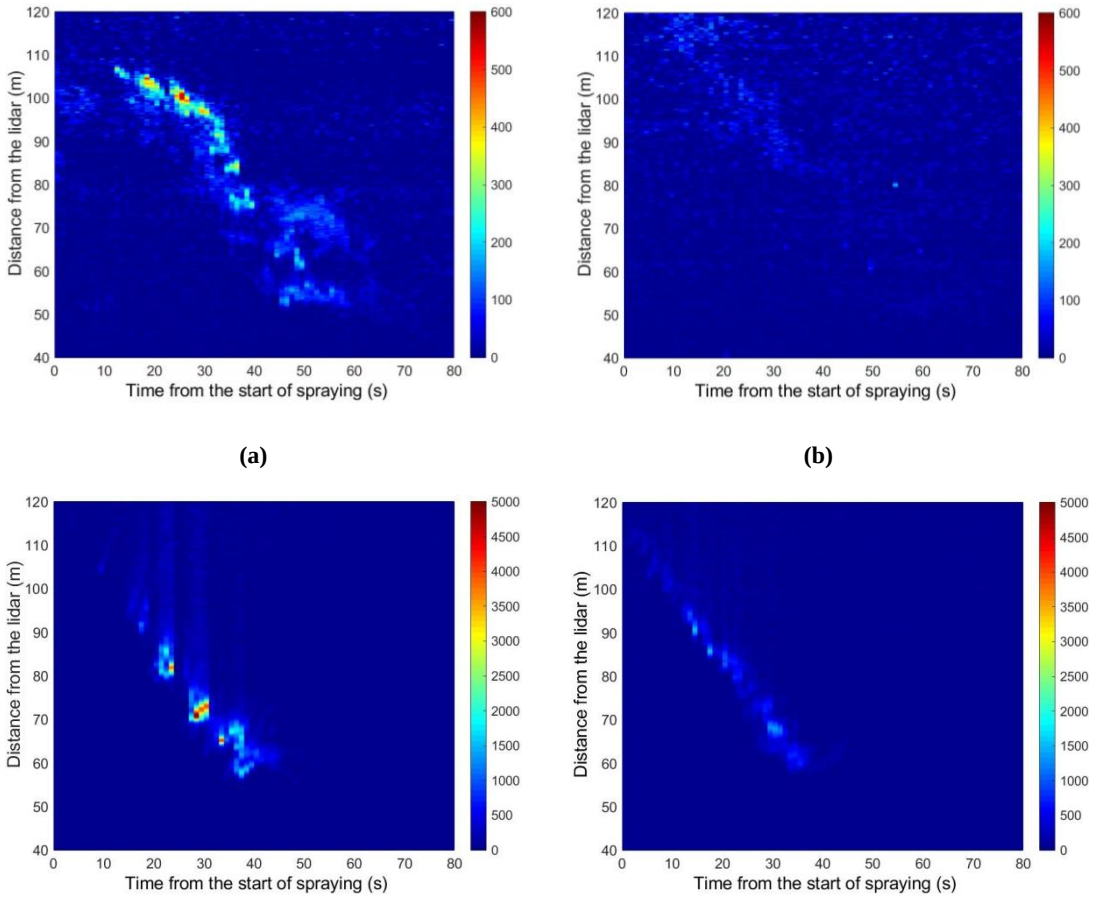

Fig. 10. LiDAR field measurements of dust and spray drift. (a) Test F1: dust raised under dry soil conditions; (b) Test F2: dust raised under wet soil conditions; (c) Test F3: spray drift, STN ATR 80 Grey at 1000 kPa; (d) Test F4: spray drift, DRN TVI 8003 Blue at 1000 kPa. Temporal resolution of 1 s and range resolution of 2.4 m. Color bar represents range-corrected backscattered signal (arbitrary units: a.u.). Signal range in (a-b) is 0-600 a.u.; in (c-d) is 0-5000 a.u.

In a second phase (tests F3 and F4), the effect of nozzle type was evaluated (STN ATR 80 Grey, Fig. 10c; DRN TVI 8003 Blue, Fig. 10d) at a pressure of 1000 kPa, under wet soil conditions. The differences in signal intensity between the two nozzle types can be observed, with signal intensity being considerably higher in the case of the STN. A *DPR* of 56.67% was obtained from a comparison between the DRN and the STN, a value lower than that obtained in the T5 and T6 spray drift potential tests (87.70%).

4. Discussion

In this work, the ability of the LiDAR system to differentiate the spray drift generated by different nozzle types and sizes has been demonstrated. The LiDAR system, as well as the PDPA, verified that DRN nozzles present a high DPR when compared to the STN. The differences obtained between the DPR_{V100} and DPR_{lidar} values (Table 5), obtained with both methods, can be attributed to the way in which the two parameters were computed. Thus, while the DPR_{lidar} was based on direct LiDAR measurements of the spray drift cloud under outdoor conditions, the DPR_{V100} was determined under controlled laboratory conditions from an indirect indicator of the drift potential (V_{100}).

Some of the nozzles used in this work were evaluated in previous studies applying other methodologies. Zande et al. (2008) classified the TVI 8001 Orange and TVI 8003 Blue nozzles in the 90% reduction class, using also as reference the ATR 80 Lilac nozzle at 700 kPa. The same class was obtained in our work when using the LiDAR measurements of these nozzles (T14, T21 and T23), with DPR_{lidar} values of 92.03% and 96.71%, respectively. In another study, Torrent et al. (2017) used a wind tunnel for the drift potential assessment of the ATR 80 Grey and TVI 8003 Blue nozzles at 1000 kPa, according to ISO 22856:2008, obtaining a *DPR* of 77.06% for airborne drift. In our work, the DPR_{V100} and DPR_{lidar} values were 98.92% and 87.70% (T5 vs. T6, Table 5), respectively. The value obtained using the LiDAR system was therefore in an intermediate position between the results obtained with the two classical methodologies (wind tunnel, PDPA).

Regarding the nozzle size comparison presented in Fig. 7, the LiDAR system was able to group the nozzles from the mean values of the LiDAR signal (drift potential) corresponding to the different nozzle sizes. As shown in Fig. 8, DPR values based on LiDAR increased with the nozzle size in accordance to the results obtained with the PDPA. The same trend was observed by Nuyttens et al. (2009) in the case of flat-fan nozzles evaluated by means of wind tunnel tests.

The results shown in Table 7 allows to state that V_{100} is the droplet size parameter that presents the best correlation with LiDAR measurements. This finding is in agreement with Arvidsson et

al. (2011) who, by means of field tests carried out with flat-fan nozzles, determined that the best spray drift potential indicator is V_{100}. Similarly, Gil et al. (2014) obtained good correlations between several droplet size parameters and the drift potential values measured by an alternative methodology and also concluded that the V_{100} was the best indicator.

Regarding LiDAR field measurements of spray drift, factors such as the sprayer forward speed or the presence of the crop could explain the resulting lower DPR values compared with those obtained in drift potential tests. In a previous field experiment, Torrent et al. (2017) also assessed the same two nozzles using vertical collectors and horizontal collectors according to ISO 22866:2005. The LiDAR measurements can be compared with those obtained with the vertical collector located at a distance of 5 m from the first tree row. In this case, the *DPR* value obtained with the vertical collector (63.82%) is in agreement with the results presented in our study (56.67%).

The results of this work reveal the capacity of the LiDAR system, compared to in situ collectors, to measure the time period that the droplets are suspended in the air. This is an important parameter for drift potential assessment, as the risk of spray drift increases with the period of suspension (Maybank et al., 1978). Until now, the lack of availability of suitable sensors meant it was not possible to measure this time.

This study has determined the drift potential reduction values for specific nozzle types and sizes using a LiDAR system, although not all of them have been verified under field conditions. Therefore, in future works, it could be interesting to test more hollow-cone nozzle models in tree crops. The difficulties associated with dust in field measurements can be solved by wetting the soil prior to the start of a spray drift study. Another way to minimize this disturbance, is to use a polarization LiDAR system capable of discriminating between dust and spray drift as proposed by Gregorio et al. (2018).

5. Conclusions

In this work, LiDAR technology is applied for the first time to compare different spray nozzles based on their drift potential reduction. In spray drift potential tests, the LiDAR system was able to differentiate and classify hollow-cone nozzles according to their type (STN, DRN) and size. Likewise, the drift potential reduction of different STN nozzles was studied, observing a progressive increase with nozzle size. The ability of the LiDAR system to discriminate between nozzle sizes with statistical validity was proved. LiDAR measurements were also contrasted with droplet size parameters, obtaining a good correlation with the V_{100}. An excellent correlation (R=0.956) was also observed when comparing the drift potential reductions calculated from LiDAR measurements with those determined from the V_{100}. In addition, LiDAR-based drift potential reduction values showed a similar trend to those determined in wind tunnel tests for sedimenting and airborne depositions.

In the field tests, it was shown that the limitation of spray drift LiDAR measurement distortion as the result of the presence of air-suspended dust can be overcome by wetting the soil before the start of the test. Moreover, the capacity of the LiDAR system to differentiate between STN and DRN under real field conditions was verified.

This work demonstrates the capacity of the LiDAR system to evaluate the spray drift potential reduction and to perform spray drift field measurements, obtaining results comparable to those of other drift assessment methodologies. LiDAR technology not only enables significant reductions in time and labor costs, it also allows observation in real time of the behavior of the drift cloud and, ultimately, an approach to spray drift studies from a more comprehensive perspective.

Acknowledgements

This work was partly funded by the Secretaria d'Universitats i Recerca del Departament d'Empresa i Coneixement de la Generalitat de Catalunya, the Spanish Ministry of Economy and Competitiveness and the European Regional Development Fund (ERDF) under Grants 2017 SGR 646, AGL2007-66093-C04-03, AGL2010-22304-04-C03-03, and AGL2013-48297-C2-2-R.

Universitat de Lleida is thanked for Mr. X. Torrent's pre-doctoral fellowship. The authors would like to thank the Unité Mixte de Recherche Information & Technologies for AgroProcess (IRSTEA, Montpellier), and particularly Jean-Paul Douzals and Cyril Tinet for the nozzle characterization using their PDPA. Our thanks are also given to the Institut de Recerca en Tecnologia Agrària (IRTA) for allowing the use of their experimental fields, and to Vicenç Maquinària Agrícola for providing the tractor. The authors also wish to thank A. Checa (Randex Iberica, S.L.) for giving us free Albuz nozzles for the spray tests. R. Lavilla, E. Ordoño and F. Solanelles are acknowledged for their assistance in the field work, and J. Arnó is thanked for his help with statistical analysis.

References

Arvidsson, T., Bergstrom, L., Kreuger, J., 2011. Spray drift as influenced by meteorological and technical factors. Pest Manage. Sci. 67, 586–598. https://doi.org/10.1002/ps.2114.

Balsari, P., Marucco, P., Tamagnone, M., 2007. A test bench for the classification of boom sprayers according to drift risk. Crop Prot. 26, 1482–1489. https://doi.org/10.1016/j.cropro.2006.12.012.

Bueno, M.R., Cunha, J.P.A.R. d., Santana, D.G. d., 2017. Assessment of spray drift from pesticide applications in soybean crops. Biosyst. Eng. 154, 35–45. https://doi.org/10.1016/j.biosystemseng.2016.10.017.

Butler Ellis, M.C., Alanis, R., Lane, A.G., Tuck, C.R., Nuyttens, D., van de Zande, J.C., 2017a. Wind tunnel measurements and model predictions for estimating spray drift reduction under field conditions. Biosyst. Eng. 154, 25-34. http://dx.doi.org/10.1016/j.biosystemseng.2016.08.013.

Butler Ellis, M.C., van den Berg, F., van de Zande, J.C., Kennedy, M.C., Charistou, A.N., Arapaki, N.S., Butler, A.H., Machera, K.A., Jacobs, C.M., 2017b. The BROWSE model for predicting exposures of residents and bystanders to agricultural use of pesticides:

519 Comparison with experimental data and other exposure models. Biosyst. Eng., 2017, 122-
520 136. http://dx.doi.org/10.1016/j.biosystemseng.2016.09.002.

521 Damalas, C.A., 2015. Pesticide drift: Seeking reliable environmental indicators of exposure
522 assessment. In: Armon, R.H., Hänninen, O. (Eds.), Environmental Indicators. Springer,
523 Dordrecht Heidelberg New York London, pp. 251–261.

524 de Jong, F.M.W., de Snoo, G.R., van de Zande, J.C., 2008. Estimated nationwide effects of
525 pesticide spray drift on terrestrial habitats in the Netherlands. J. Environ. Manage. 86, 721–
526 730. https://doi.org/10.1016/j.jenvman.2006.12.031.

527 De Schampheleire, M., Spanoghe, P., Brusselman, E., Sonck, S., 2007. Risk assessment of
528 pesticide spray drift damage in Belgium. Crop. Prot. 26, 602–611.
529 https://doi.org/10.1016/j.cropro.2006.05.013.

530 EPA - United States Environmental Protection Agency, n.d. Introduction to pesticide drift
531 [WWW Document]. URL https://www.epa.gov/reducing-pesticide-drift/introduction-
532 pesticide-drift (accessed 8.18.18).

533 Felsot, A.S., Unsworth, J.B., Linders, J.B.H.J., Roberts, G., Rautman, D., Harris, C., Carazo, E.,
534 2010. Agrochemical spray drift; assessment and mitigation-A review. J. Environ. Sci. Heal.
535 Part B 46, 1–23. https://doi.org/10.1080/03601234.2010.515161.

536 Ferguson, J.C., O'Donnell, C.C., Chauhan, B.S., Adkins, S.W., Kruger, G.R., Wang, R., Ferreira,
537 P.H.U., Hewitt, A.J., 2015. Determining the uniformity and consistency of droplet size
538 across spray drift reducing nozzles in a wind tunnel. Crop Prot. 76, 1-6.
539 http://dx.doi.org/10.1016/j.cropro.2015.06.008.

540 FOCUS, 2004. Landscape and mitigation factors in aquatic risk assessment. Volume 1: extended
541 summary and recommendations. Report of the FOCUS Working Group on landscape and
542 mitigation factors in ecological risk assessment.

543 Ganzelmeier, H., Rautmann, D., Spangenberg, R., Streloke, M., Herrmann, M., Wenzelburger,

544 H.J., Walter., H.F., 1995. Studies on the spray drift of plant protection products: Results of
545 a test program carried out throughout the Federal Republic of Germany. Blackwell, Berlin.

546 Garcerá, C., Moltó, E., Chueca, P., 2017. Spray pesticide applications in Mediterranean citrus
547 orchards: Canopy deposition and off-target losses. Sci. Total Environ. 599-600, 1344-1362.
548 http://dx.doi.org/10.1016/j.scitotenv.2017.05.029.

549 Gil, E., Balsari, P., Gallart, M., Llorens, J., Marucco, P., Andersen, P.G., Fàbregas, X., Llop, J.,
550 2014. Determination of drift potential of different flat fan nozzles on a boom sprayer using
551 a test bench. Crop Prot. 56, 58–68. https://doi.org/10.1016/j.cropro.2013.10.018.

552 Gil, E., Balsari, P., Marucco, P., Pilar, M., 2015. Influence of wind velocity and wind direction
553 on measurements of spray drift potential of boom sprayers using drift test bench. Agric. For.
554 Meteorol. 202, 94–101. https://doi.org/10.1016/j.agrformet.2014.12.002.

555 Gil, E., Llorens, J., Gallart, M., Gil-Ribes, J.A., Miranda-Fuentes, A., 2018. First attempts to
556 obtain a reference drift curve for traditional olive grove's plantations following ISO 22866.
557 Sci. Total Environ. 627, 349–360. https://doi.org/10.1016/j.scitotenv.2018.01.229.

558 Gil, Y., Sinfort, C., 2005. Emission of pesticides to the air during sprayer application : A
559 bibliographic review 39, 5183–5193. https://doi.org/10.1016/j.atmosenv.2005.05.019.

560 Gregorio, E., Gené, J., Sanz, R., Rocadenbosch, F., Chueca, P., Arnó, J., Solanelles, F., Rosell-
561 Polo, J.R., 2018. Polarization lidar detection of agricultural aerosol emissions. J. Sensors
562 (Switzerland), 1–9. https://doi.org/10.1155/2018/1864106.

563 Gregorio, E., Rocadenbosch, F., Sanz, R., Rosell-Polo, J.R., 2015. Eye-Safe lidar system for
564 pesticide spray drift measurement. Sensors (Switzerland) 15, 3650-3670.
565 https://doi.org/10.3390/s150203650.

566 Gregorio, E., Rosell-Polo, J.R., Sanz, R., Rocadenbosch, F., Solanelles, F., Garcerà, C., Chueca,
567 P., Arnó, J., del Moral, I., Masip, J., Camp, F., Viana, R., Escolà, A., Gràcia, F., Planas, S.,
568 Moltó, E., 2014. LIDAR as an alternative to passive collectors to measure pesticide spray

drift. Atmos. Environ. 82, 83–93.

Gregorio, E., Torrent, X., Planas, S., Solanelles, F., Sanz, R., Rocadenbosch, F., Masip, J., Ribes-Dasi, M., Rosell-Polo, J.R., 2016. Measurement of spray drift with a specifically designed lidar system. Sensors (Switzerland) 16, 499. https://doi.org/10.3390/s16040499.

Grella, M., Marucco, P., Balsari, P., 2019. Toward a new method to classify the airblast sprayers according to their potential drift reduction: comparison of direct and new indirect measurement methods. Pest Manag. Sci. (in press). https://doi.org/10.1002/ps.5354.

Heidary, M. Al, Douzals, J.P., Sinfort, C., Vallet, A., 2014. Influence of spray characteristics on potential spray drift of field crop sprayers : A literature review. Crop Prot. 63, 120–130. https://doi.org/10.1016/j.cropro.2014.05.006.

Hiscox, A.L., Miller, D.R., Nappo, C.J., Ross, J., 2006. Dispersion of fine spray from aerial applications in stable atmospheric conditions. Trans. ASABE 49, 1513–1520.

Hoff, R.M., Mickle, R.E., Froude, F.A., 1989. A rapid acquisition lidar system for aerial spray diagnostics. Trans. ASAE 32(5), 1523-1528.

Holterman, H.J., van de Zande, J.C., Huijsmans, J.F.M., Wenneker, M., 2017. An empirical model based on phenological growth stage for predicting pesticide spray drift in pome fruit orchards. Biosyst. Eng. 154, 46-61. http://dx.doi.org/10.1016/j.biosystemseng.2016.08.016.

Holterman, H., van de Zande, J.C., Porskamp, H.A., Huijsmans, J.F., 1997. Modelling spray drift from boom sprayers. Comput. Electron. Agric. 19, 1–22. https://doi.org/10.1016/S0168-1699(97)00018-5.

ISO 22401, 2015. Equipment for crop protection - Method for measurement of potential spray drift from horizontal boom sprayers by the use of a test bench. International Organization for Standardization, Geneva.

593 ISO 22856, 2008. Equipment for crop protection - Methods for the laboratory measurement of
594 spray drift - Wind tunnels. International Organization for Standardization, Geneva.

595 ISO 22866, 2005. Equipment for crop protection - Methods for field measurement of spray drift.
596 International Organization for Standardization, Geneva.

597 ISO 25358, 2018. Crop protection equipment - Droplet-size spectra from atomizers -
598 Measurement and classification. International Organization for Standardization, Geneva.

599 Khot, L.R., Miller, D.R., Hiscox, A.L., Salyani, M., Walker, T.W., Farooq, M., 2011.
600 Extrapolation of droplet catch measurements in aerosol application treatments. At. Sprays
601 21, 149–158. https://doi.org/10.1615/AtomizSpr.2011002846.

602 Maybank, J., Yoshida, K., Grover, R., 1978. Spray drift from agricultural pesticide applications.
603 J. Air Pollut. Control Assoc. 28, 1009–1014.
604 https://doi.org/10.1080/00022470.1978.10470699.

605 Measures, R.M., 1992. Laser Remote Sensing: Fundamentals and Applications. Krieger
606 Publishing Company, Malabar, Florida.

607 Miller, P., 2014. Spray drif, in: Matthews, G.A., Bateman, Roy, Miller, Paul (Ed.), Pesticide
608 Application Methods, Wiley Online Books, pp. 337–361.
609 https://doi.org/doi:10.1002/9781118351284.ch12.

610 Nuyttens, D., 2007. Drift from field crop sprayers: The influence of spray application technology
611 determined using indirect and direct drift assessment means. PhD thesis nr. 772, KU Leuven.
612 293 p. ISBN 978-908826-039-1. Katholieke Universiteit Leuven - Faculteit Bio-
613 ingenieurswetenschappen. https://doi.org/10.1017/CBO9781107415324.004.

614 Nuyttens, D., De Schampheleire, M., Verboven, P., Sonck, B., 2010. Comparison between
615 indirect and direct spray drift assessment methods. Biosyst. Eng. 105, 2–12.
616 https://doi.org/10.1016/j.biosystemseng.2009.08.004.

617 Nuyttens, D., Taylor, W.A., De Schampheleire, M., Verboven, P., Dekeyser, D., 2009. Influence
618 of nozzle type and size on drift potential by means of different wind tunnel evaluation
619 methods. Biosyst. Eng. 103, 271–280.
620 https://doi.org/10.1016/j.biosystemseng.2009.04.001.

621 Nuyttens, D., Zwertvaegher, I.K.A., Dekeyser, D., 2017. Spray drift assessment of different
622 application techniques using a drift test bench and comparison with other assessment
623 methods. Biosyst. Eng. 154, 14–24. https://doi.org/10.1016/j.biosystemseng.2016.09.013.

624 Otto, S., Loddo, D., Baldoin, C., Zanin, G., 2015. Spray drift reduction techniques for vineyards
625 in fragmented landscapes. J. Environ. Manage. 162, 290–298.
626 https://doi.org/10.1016/j.jenvman.2015.07.060.

627 Rautmann, D., Streloke, M., Winkler, R., 2001. New basic drift values in the authorization
628 procedure for plant protection products. Mitt. Biol. Bundesanst. Land Forstwirtsch 383,
629 133–141.

630 Stoughton, T.E., Miller, D.R., Yang, X., Ducharme, K.M., 1997. A comparison of spray drift
631 predictions to lidar data. Agric. For. Meteorol. 88, 15–26. https://doi.org/10.1016/S0168-
632 1923(97)00056-7.

633 Taylor, W.A., Womac, A.R., Miller, P.C.H., Taylor, B.P., 2004. An Attempt to Relate Drop Size
634 to Drift Risk, in: International Conference on Pesticide Application for Drift Management
635 Octobre 27-29. pp. 210–223.

636 Torrent, X., Garcerá, C., Moltó, E., Chueca, P., Abad, R., Grafulla, C., Román, C., Planas, S.,
637 2017. Comparison between standard and drift reducing nozzles for pesticide application in
638 citrus: Part I. Effects on wind tunnel and field spray drift. Crop Prot. 96, 130–143.
639 https://doi.org/10.1016/j.cropro.2017.02.001.

640 Torrent, X., Gregorio, E., Douzals, J.P., Rosell-Polo, J.R., Planas, S., 2019. Assessment of spray
641 drift for hollow-cone nozzles: Part 1. Indirect methods comparison. Sci. Total Environ.

642 (accepted).

643 Van de Zande, J.C., Holterman, H.J., Wenneker, M., 2008. Nozzle classification for drift
644 reduction in orchard spraying: Identification of drift reduction class threshold nozzles.
645 Agricultural Engineering International: the CIGR Ejournal. Manuscript ALNARP 08 0013.
646 Vol. X.

647 Wandinger, U., 2005. Introduction to Lidar, in: Weitkamp, C. (Ed.), Lidar. Range-Resolved
648 Optical Remote Sensing of the Atmosphere. Springer-Verlag, pp. 1–18.
649 https://doi.org/10.1007/0-387-25101-4_1.

650 Zhang, X., Luo, Y., Goh, K.S., 2018. Modeling spray drift and runoff-related inputs of pesticides
651 to receiving water. Environ. Pollut. 234, 48–58.
652 https://doi.org/10.1016/j.envpol.2017.11.032.